Prediction of cutting forces from an analytical model of oblique cutting, application to peripheral milling of Ti-6Al-4V alloy — Source link ↗

A. Moufki, D. Dudzinski, G. Le Coz

Institutions: University of Lorraine

Related papers:

- Manufacturing Automation: Metal Cutting Mechanics, Machine Tool Vibrations, and CNC Design

- Analytical prediction of cutting forces in orthogonal cutting using unequal division shear-zone model

- Mechanics of the Metal Cutting Process. I. Orthogonal Cutting and a Type 2 Chip

- An analytical model of oblique cutting with application to end milling

- The Mechanics of Machining: An Analytical Approach to Assessing Machinability

Prediction of milling forces from an oblique cutting thermomechanical model, application to peripheral milling of Ti-6Al-4V alloy

A. Moufki, D. Dudzinski, Gael Le Coz

Prediction of milling forces from an oblique cutting thermomechanical model, application to peripheral milling of Ti-6Al-4V alloy

A. Moufki, D. Dudzinski, G. Le Coz
Laboratoire d'Etudes des Microstructures et de la Mécanique des Matériaux
LEM3 UMR CNRS 7239
Université de Lorraine, Ile du Saulcy, 57045 Metz France

Abstract.

In this work, a predictive machining theory, based on an analytical thermomechanical approach of oblique cutting, Moufki et al. [18, 19], is applied to the peripheral milling process. The material characteristics such as strain rate sensitivity, strain hardening and thermal softening are considered. In the primary shear zone, thermomechanical coupling and inertia effects are accounted for. The present analytical approach leads to a three dimensional cutting force model for end milling operations. Calculated and experimental results are compared for several operations: full immersion, up-milling and down-milling and for different cutting conditions. The proposed model appears as an interesting alternative to the mechanistic approach which requires many experimental tests to determine the milling cutting force coefficients.

Nomenclature

ω angular velocity

α_h helix angle

α_r radial angle

α_n normal rake angle

R tool radius

N_t number of teeth

V cutting speed $(V = \omega R)$

φ_i angular position for the ith tooth

φ_{en} entrance angle

φ_{out} exit angle

η_s angle determining the x_s-direction

η_c chip flow angle

d_r radial depth of cut

d_a axial depth of cut

f_t feed rate per tooth

z axial position for a point cutting edge

t_1 undeformed chip thickness

λ_s edge inclination angle

h primary shear zone thickness

ϕ_n normal shear angle

$\bar{\mu}$ mean (or apparent) friction coefficient at the rake face

λ mean (or apparent) friction angle ($\bar{\mu} = \tan(\lambda)$)

x_s, y_s, z_s coordinate system fixed with the primary shear zone

x_s coordinate along the shearing direction

z_s coordinate along the normal direction to the primary shear band

$\boldsymbol{\sigma}$ Cauchy stress tensor

$\boldsymbol{\Gamma}_R$ relative acceleration vector

$\boldsymbol{\Gamma}_{Co}$ Coriolis acceleration vector

$\boldsymbol{\Gamma}_C$ centripetal acceleration vector

τ shear stress

γ shear strain

$\dot{\gamma}$ shear strain rate

T temperature

T_w workpiece temperature

n hardening exponent

m strain rate sensitivity

ν thermal softening coefficient

$A, B, \dot{\gamma}_0$ constant material characteristics (Johnson-Cook law)

ρ, c, k material density, heat capacity and heat conductivity coefficient

β Taylor-Quinney coefficient

$d\mathbf{R}_{tool/chip}$ elementary cutting force exerted on the chip element by the tool

dF_f, dN_f elementary friction and normal forces exerted on the chip element by the rake face

dF_t, dF_r, dF_a elementary cutting, thrust and lateral forces exerted on the chip element by the tool

K_{tc}, K_{rc}, K_{ac} cutting force coefficients

K_{te}, K_{re}, K_{ae} edge force coefficients

1 - Introduction

The end milling is commonly used in aerospace industry and in dies and moulds manufacturing. Various unfavourable conditions can affect the machined surface quality during end milling, such as excessive cutter deflection, machine tool chatter, tool wear, and cutter breakage. To optimize the machining process, it is necessary to reduce the cutting forces and the cutting temperatures in order to achieve the surface quality requirements with an acceptable tool life. Due to the complexity of manufacturing processes, empirical approaches are often used to determine machining parameters for instance tool selection, cutting speeds and feed rates. This leads frequently to sub-optimal solutions. Therefore, a predictive model of cutting forces may be very useful for the cutting process optimisation.

As recalled by Budak et al. [1], the prediction of cutting forces during machining processes is usually established by using semi-empirical or mechanistic approaches. The forces are calculated from the chip load and by using force coefficients determined experimentally from machining tests for a given cutter geometry and a tool-workpiece pair.

In the particular case of milling operations, the radial depth of cut varies continuously; Martelotti [2] studied the geometry of milling and proposed a simplified formula to calculate the instantaneous undeformed or uncut chip thickness. Koenigsberger and Sabberwal [3] analysed tangential forces and they found a strong influence of the average chip thickness on these variables. Tlusty and MacNeil [4] Kline et al. [5], Kline and DeVor [6] used average milling force coefficients and presented discrete milling force model. In their approach, the end milling process is examined by discretizing it angle by angle, flute by flute; and finally, after dividing the end mill into axial segments, slice by slice, as explained by Sutherland and DeVor [7]. At each angular position, they calculated the total cutting forces by integration. Altintas and Spence [8] presented closed form expressions to calculate the helical end milling forces more accurately and Yucesan and Altintas [9] developed a mechanistic model by including the influence of instantaneous chip thickness and rake angles into the milling force coefficients.

As noted by Budak et al. [1] despite the sophistication and usefulness of the mechanistic models, their predictive capability depends on the empirically established milling force coefficients determined for each cutter design and for each tool-workpiece materials combination. A large amount of milling tests are then necessary and this approach appears to be costly and not appropriate for process planers and tool designers; and finally it corresponds more to a calibration procedure than to a really predictive approach. Today, the mechanistic approach is still employed with some refinements, see for example Dang et al. [10], Wang et al. [11].

An alternative way to determine the milling cutting force coefficients is to use an orthogonal cutting data base and the oblique cutting analysis associated to the milling process; that was the method chosen by Armarego et al. [12, 13, 14]. A comparison between the two previous methods for the prediction of milling forces was done by Budak et al. [1].

Another possibility is to apply the Oxley's predictive orthogonal cutting theory extended to oblique cutting, Oxley [15]. Li and Li [16, 17] developed such an approach and determined the end milling forces along the working cutting edges. It must be noted that in this approach, a sticking contact independent of the tool material was assumed at the tool-chip interface. In addition, the predictive machining theory uses several empirical relations whose coefficients have to be determined.

According to the fact that along an engaged cutting edge of an end mill, the cutting process is an oblique one with an angle of obliquity equal to the helix angle, the present paper proposes to apply the thermomechanical model of oblique cutting developed by Moufki et al. [18, 19] to calculate the end milling forces. That leads to a three dimensional predictive cutting force model for end milling operations. The input parameters are the worked material thermomechanical characteristics, the tool-chip interface friction coefficient, and the cutting conditions. Using the proposed predictive model, milling forces are determined for various cutting conditions and different tool geometries during peripheral milling of a titanium alloy; they are compared to experimental results.

2 – Geometric model of milling process

The end milling operation is analyzed with respect to the frame (x, y, z) as shown in Fig. 1.

At axial position z, an axial elemental disk of thickness dz is considered. For the ith cutting tooth, the angular position at time t is given by :

$$\varphi_i(z) = \omega t - \frac{z}{R}\tan\alpha_h + (i-1)\frac{2\pi}{N_t} \tag{1}$$

where N_t is the number of teeth of the end mill, $\omega\,(rad/s)$ the angular velocity, α_h the helix angle and R the tool radius. The angular position measured clockwise are considered as positive. For the present model, tool wear and tool vibrations are not taken into account; then, only one tool rotation is useful for the simulation and it is the reason why the time is limited to $t \in [0, 2\pi/\omega]$.
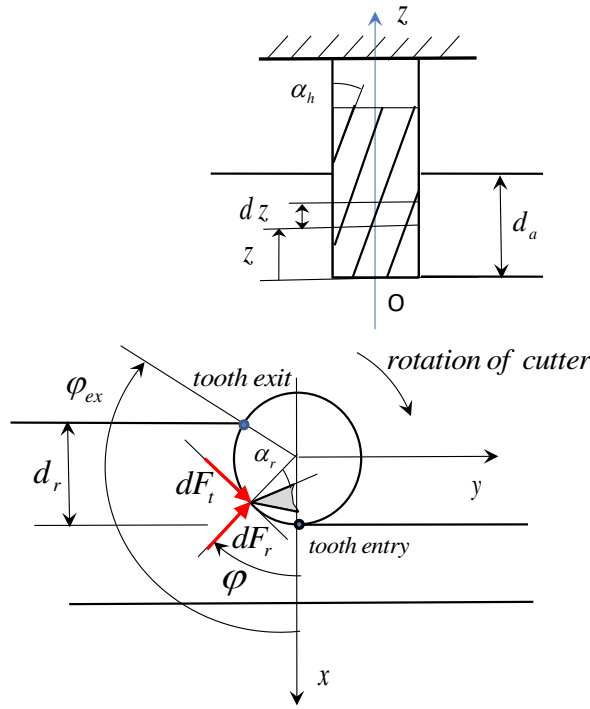

Fig. 1. Peripheral milling process.

If φ_{en} is the angle at which the cutter enters the cut, and φ_{ex} the angle at which the cutter exits the cut, they are defined as follows :

$$
\begin{aligned}
&\varphi_{en} = 0 \quad \text{and} \quad \varphi_{ex} = \pi && \text{for slot milling (full immersion)} \\
&\varphi_{en} = 0 \quad \text{and} \quad \varphi_{ex} = \cos^{-1}(1 - d_r/R) && \text{for up-milling} \\
&\varphi_{en} = \pi/2 + \sin^{-1}(1 - d_r/R) \quad \text{and} \quad \varphi_{ex} = \pi && \text{for down-milling}
\end{aligned}
\tag{2}
$$

where d_r is the radial depth of cut, Fig. 1.

The end mill cuts the workpiece when :

$$\varphi_{en} < \varphi_i(z=0) < \left(\varphi_{ex} + \frac{d_a}{R}\tan\alpha_h\right) \tag{3}$$

where d_a is the axial depth of cut, Fig. 1. Note that the conditions (2) and (3) require that $0 \leq \varphi_i(z=0) \leq 2\pi$. Thus if $\varphi_i(z) \geq 2k\pi$ (k is an integer), the value of $\varphi_i(z)$ is replaced by $\varphi_i(z) - 2k\pi$.

3 – Prediction of milling force coefficients from a thermomechanical oblique cutting model

3.1 – oblique cutting in milling

For an elemental disk of thickness *dz*, the ith cutting edge element supposed as linear produces a chip element under oblique cutting conditions, Fig. 2. The cutting edge inclination angle *λs* is equal to the helix angle α_h, all along the cutting edge ; only the chip thickness changes from one cutting element to another. The chip thickness is given by :

$$t_1 = f_t \sin(\varphi_i) \tag{4}$$

where f_t is the feed rate per tooth. The normal rake angle α_n is obtained from the radial angle α_r and the helix angle α_h:

$$\alpha_n = \tan^{-1}(\tan\alpha_r \ \cos\alpha_h) \tag{5}$$

and the cutting velocity is $V = R\,\omega$.
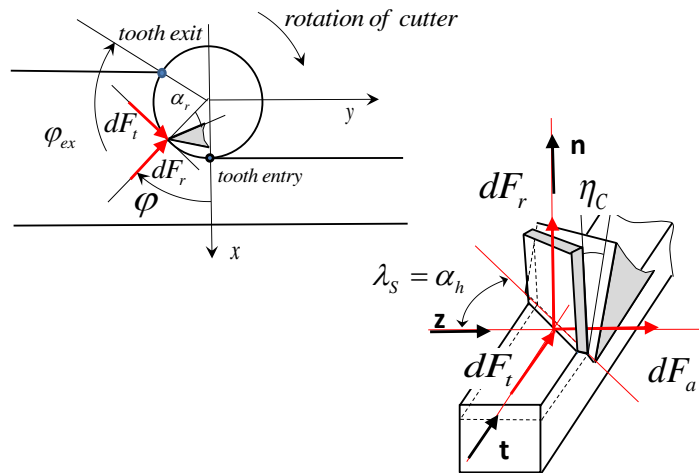

Fig. 2. Peripheral milling and the associated oblique cutting process for a cutting element of the end mill; t and n are the unit vectors of the circumferential and radial directions, respectively.

This oblique cutting process is modelled by using the thermomechanical approach of oblique cutting developed previously by Moufki et al. [18, 19]. Although this predictive

machining theory was established for stationary conditions, it may be applied to milling operations by using the assumption that at each instant of time the chip formation is modelled by an equivalent stationary process, as it was postulated by Li and Li [16, 17].

The primary shear zone is assumed to be a shear band of constant thickness h, as shown in Fig. 3. The deformation in the chip is supposed to be limited to this band which is characterized by the normal shear angle ϕ_n measured in the plane P_n perpendicular to the cutting edge element, see Fig. 3. The secondary shear deformation at the tool-chip interface and the complex material flow at the vicinity of the tool edge are not considered. However, as shown later the contact conditions between the tool and the chip may be taken into account through: (i) the mean friction coefficient $\bar{\mu}$ along the rake face; and (ii) the cutting edge effect through the edge force coefficients K_{te}, K_{re} and K_{ae}. The thermomechanical properties of the work material and the inertia effects are accounted for to describe the material flow in the primary shear zone. On the tool rake face, the chip flow angle η_c is determined from an implicit equation which is deduced from the chip equilibrium by assuming that the friction force is collinear to the chip flow direction. The analysis is limited to stationary flow (no time dependence) and the material flow within the primary shear zone is modelled by using a one-dimensional approach. Therefore, all the variables describing the material flow depend only on the coordinate z_s along the normal to the band, Fig. 3. In addition, the shearing in the band is supposed to be adiabatic. This assumption is reasonable when the cutting speed is large enough or when the material heat conductivity is low, such as for the titanium alloy. The input parameters of the model are : the cutting conditions, the thickness h, the normal shear angle ϕ_n and the mean friction coefficient $\bar{\mu}$ at the rake face.
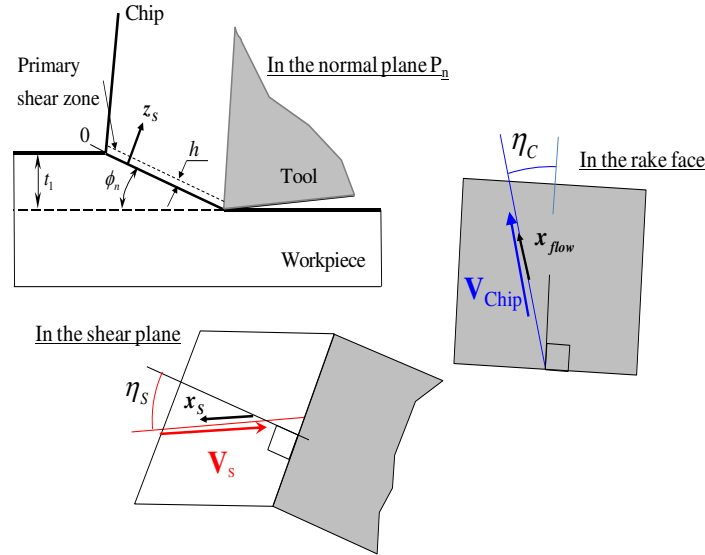
Fig. 3. Oblique cutting process. Shear velocity V_S, chip flow velocity V_Chip, cutting speed V is along the circumferential direction t, Fig. 2.

The material flow through the primary shear zone is analysed with respect to a frame reference (x_s, y_s, z_s) associated to the shear band. This frame moves with the tool having a trajectory which results from the tool rotational motion.

The frame (x_s, y_s, z_s) is a non-inertial frame, and the equation of motion for a material particle in the primary shear zone takes the following form:

$$\nabla \cdot \boldsymbol{\sigma} - \rho\left(\boldsymbol{\Gamma}_{\mathrm{Co}} + \boldsymbol{\Gamma}_{\mathrm{C}}\right) = \rho\,\boldsymbol{\Gamma}_{\mathrm{R}} \tag{6}$$

Where $\boldsymbol{\sigma}$ is the Cauchy stress tensor; $\boldsymbol{\Gamma}_{\mathrm{R}}$ the relative acceleration vector measured in the rotating frame (x_s, y_s, z_s); $\boldsymbol{\Gamma}_{\mathrm{Co}}$ the Coriolis acceleration and $\boldsymbol{\Gamma}_{\mathrm{C}}$ the centripetal acceleration.

To evaluate the different acceleration terms, scale analysis is used :

$$\left|\boldsymbol{\Gamma}_{\mathrm{R}}\right| \Box \frac{V^2}{h} ; \quad \left|\boldsymbol{\Gamma}_{\mathrm{C}}\right| \Box \omega^2 R ; \quad \left|\boldsymbol{\Gamma}_{\mathrm{Co}}\right| \Box \omega V \tag{7}$$

Then :

$$\frac{\left|\boldsymbol{\Gamma}_{\mathrm{R}}\right|}{\left|\boldsymbol{\Gamma}_{\mathrm{Co}}\right|} \Box \frac{R}{h}, \quad \frac{\left|\boldsymbol{\Gamma}_{\mathrm{R}}\right|}{\left|\boldsymbol{\Gamma}_{\mathrm{C}}\right|} \Box \frac{R}{h} \tag{8}$$

R and h represent respectively the end mill radius and the thickness of the primary shear zone. Since the ratio R/h is very weak (the shear band is a narrow zone with thickness h

of the order of few micro-meters), it is clear that the frame (x_s, y_s, z_s) associated to the shear zone may be assimilated to an inertial frame; the Coriolis and the centripetal accelerations are negligible.

3.2 - Oblique cutting model equations:

The worked material is supposed to be isotropic and rigid (the elastic deformations are neglected). The thermomechanical response is described by the following Johnson-Cook law:

$$\tau = \frac{1}{\sqrt{3}} \left[A + B \left(\frac{\gamma}{\sqrt{3}} \right)^n \right] \left[1 + m \ln \left(\frac{\dot{\gamma}}{\dot{\gamma}_0} \right) \right] \left[1 - \left(\frac{T - T_r}{T_m - T_r} \right)^v \right] \tag{9}$$

where τ, γ, $\dot{\gamma}$, and T represent respectively the shear stress, the shear strain, the shear strain rate and the temperature. The characteristics of material behaviour are the strain hardening exponent n, the strain rate sensitivity coefficient m, the thermal softening exponent v and constants A, B, $\dot{\gamma}_0$, T_r (reference temperature) and T_m (melting temperature).

The conservation of momentum in the shear band gives for the shear stress :

$$\tau = \tau(\gamma, \tau_0) = \rho \left(V \cos \lambda_s \sin \phi_n \right)^2 \gamma + \tau_0 \tag{10}$$

where ρ the material density, V the cutting velocity, λ_s the edge inclination angle, ϕ_n the normal shear angle, γ the shear strain in the band and τ_0 the stress at the entry.

The temperature in the band is obtained with the conservation of energy (assuming adiabatic conditions):

$$T = T(\gamma, \tau_0) = T_w + \frac{\beta}{\rho c} \left(\rho \left(V \cos \lambda_s \sin \phi_n \right)^2 \frac{\gamma^2}{2} + \tau_0 \gamma \right) \tag{11}$$

where β, c, T_w and τ_0 represent respectively the Taylor-Quinney coefficient, the heat capacity, the workpiece temperature and the shear stress at the entry of the primary shear zone.

The strain rate can be extracted from the constitutive law (9) and written as:

$$\dot{\gamma}(\gamma, \tau_0) = \dot{\gamma}_0 \exp \left(\frac{\tau \sqrt{3}}{g_1(\gamma) g_2(T)} - \frac{1}{m} \right) \tag{12}$$

With:

$$g_1(\gamma) = \left(A + B\left(\gamma/\sqrt{3}\right)^n \right), \quad g_2(T) = \left(1 - \left(\frac{T - T_r}{T_f - T_r} \right)^v \right) \tag{13}$$

Using the one-dimensional formulation, the material derivative of the shear strain γ is reduced to the following first order differential equation:

$$\frac{d\gamma}{dz_s} = \frac{\dot{\gamma}(\gamma, \tau_0)}{V \cos\lambda_s \sin\phi_n} \tag{14}$$

where z_s represents the material position along the normal to the shear band (one-dimensional formulation) as shown in Fig. 3.

Considering that the deformation in the chip is limited to the band, the shear strain at the entry of the shear band ($z_s = 0$) is zero and at the outflow of the shear band ($z_s = h$) we have:

$$\gamma = (z_s = h) = \gamma_h = \frac{1}{\cos\eta_s} \left(\frac{\cos\alpha_n}{\sin\phi_n \cos(\phi_n - \alpha_n)} \right) \tag{15}$$

As it has been shown in Moufki et al. [19], the angle η_s, which characterizes the shear direction in the primary shear zone, is constant in band and it is determined from:

$$\eta_s = \tan^{-1} \left(\frac{\tan\eta_c \sin\phi_n - \tan\lambda_s \cos(\phi_n - \alpha_n)}{\cos\alpha_n} \right) \tag{16}$$

with η_c is the chip flow angle on the tool rake face, Fig. 3.
Finally, the integrated form of relation (14) and the condition (15) are used to determine the stress τ_0 at the entry of the band (for $z_s = 0$) from the following non-linear equation:

$$\int_0^{\gamma_h} \frac{V \cos\lambda_s \sin\phi_n}{\dot{\gamma}(\gamma, \tau_0)} \, d\gamma - h = 0 \tag{17}$$

The normal shear angle ϕ_n is assumed to be given by a modified Merchant law:

$$\phi_n = A_1 + A_2 \left(\alpha_n - \lambda \right) \tag{18}$$

where $\lambda = \tan^{-1}(\overline{\mu})$ is the mean friction angle at the tool rake face. The constants A_1 and A_2 depend on the work material.

During cutting process, the tribological conditions between the tool and the chip are very complex with high values of pressure and temperature, see for example Bahi et al.

[20,21]. Many experimental investigations, Zorev [22], Trent [23], Ackroyd [24], Asthakov [25], have shown the existence of sticking and sliding zones along the tool rake face. Thus, due to the complexity of the tool-chip contact, the full understanding of the contact conditions has not been enough developed. Moreover, there is no model able to predict correctly the friction law along the tool rake face, Filice [26]. In the present work, to determine the cutting forces, it was sufficient to use an apparent friction coefficient $\bar{\mu}$ to take globally into account the contact conditions along the rake face. In addition, to introduce the rubbing effect at the cutting edge, edge force coefficients were employed as in the mechanistic approach of Altinas [27].
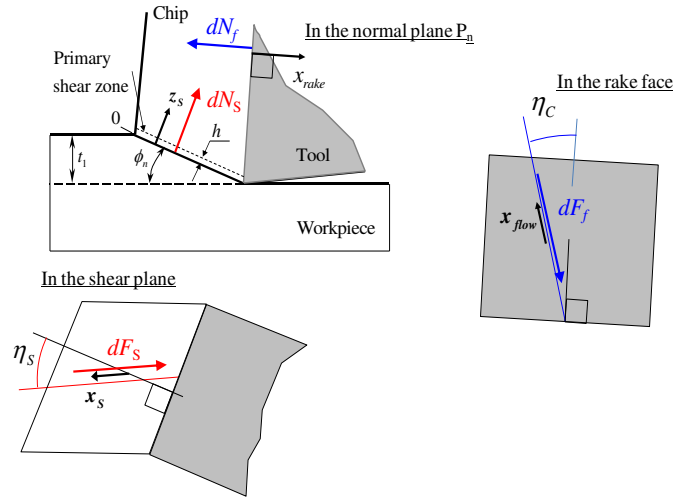

Fig. 4. Forces on an elemental chip under oblique conditions.

The elemental force exerted by the workpiece along the plane ($z_s = h$), Fig. 4, may be decomposed into two components, the first one is collinear to the shearing direction and the second one is normal to the band :

$$d\mathbf{R}_{workpiece/chip} = -dF_s\, \mathbf{x_s} + dN_s\, \mathbf{z_s} \qquad with \quad dF_s = \frac{dz\, t_1}{\cos \lambda_s \sin \phi_n} \tau_h \tag{19}$$

where τ_h is the shear stress at the exit of the band obtained from (10) and given by :

$$\tau = \rho \left(V \cos \lambda_s \sin \phi_n \right)^2 \gamma_h + \tau_0 \tag{20}$$

11

The elemental force exerted by the tool on the chip, Fig. 4, may be decomposed into two components, the first one, the frictional force, is collinear to the flow direction and the second one is normal to the rake face :

$$dR_{tool/chip} = dF_f \, \mathbf{x}_{flow} + dN_f \, \mathbf{z}_{rake} \tag{21}$$

with $dF_f = -\|dR_{tool/chip}\|\sin\lambda$ and $dN_f = -\|dR_{tool/chip}\|\cos\lambda$

From the equilibrium of the forces exerted on the elementary chip :

$$\begin{cases} \|dR_{tool/chip}\| = \dfrac{dF_s \cos\eta_s}{\cos\lambda\left(\cos(\phi_n - \alpha_n) - \tan\lambda\cos\eta_c \sin(\phi_n - \alpha_n)\right)} \\[2mm] dN_s = \|dR_{tool/chip}\|\cos\lambda\left(\sin(\phi_n - \alpha_n) + \tan\lambda\cos\eta_c \cos(\phi_n - \alpha_n)\right) \end{cases} \tag{22}$$

and the chip flow angle is calculated from the following implicit equation:

$$\begin{aligned} &\cos(\phi_n - \alpha_n)\sin\phi_n \sin\eta_c - \tan\lambda_s \cos^2(\phi_n - \alpha_n)\cos\eta_c \\ &+\left(\cos\alpha_n - \sin(\phi_n - \alpha_n)\sin\phi_n\right)\tan\lambda\sin\eta_c \cos\eta_c + \\ &\tan\lambda\tan\lambda_s \sin(\phi_n - \alpha_n)\cos(\phi_n - \alpha_n)\cos^2\eta_c = 0 \end{aligned} \tag{23}$$

Finally, the elementary cutting forces dF_t, dF_r, dF_a, exerted on a cutting element, are given by :

$$\begin{cases} dF_t = \|dR_{tool/chip}\|\cos\lambda\left(\cos\alpha_n \cos\lambda_s + \tan\lambda\left(\sin\eta_c \sin\lambda_s + \cos\eta_c \sin\alpha_n \cos\lambda_s\right)\right) \\[1mm] dF_r = \|dR_{tool/chip}\|\cos\lambda\left(-\sin\alpha_n + \tan\lambda\cos\eta_c \cos\alpha_n\right) \\[1mm] dF_a = \|dR_{tool/chip}\|\cos\lambda\left(\cos\alpha_n \sin\lambda_s + \tan\lambda\left(-\sin\eta_c \cos\lambda_s + \cos\eta_c \sin\alpha_n \sin\lambda_s\right)\right) \end{cases} \tag{26}$$

where dF_t, dF_r, dF_a correspond respectively to the cutting force, thrust force and lateral force, see Fig. 2.

Considering (22), these forces may be rewritten as :

$$dF_t = \frac{dF_s \cos\eta_s \left(\cos\alpha_n \cos\lambda_s + \tan\lambda\left(\sin\eta_c \sin\lambda_s + \cos\eta_c \sin\alpha_n \cos\lambda_s\right)\right)}{\cos(\phi_n - \alpha_n) - \tan\lambda\cos\eta_c \sin(\phi_n - \alpha_n)}$$

$$dF_r = \frac{dF_s \cos\eta_s \left(-\sin\alpha_n + \tan\lambda\cos\eta_c \cos\alpha_n\right)}{\cos(\phi_n - \alpha_n) - \tan\lambda\cos\eta_c \sin(\phi_n - \alpha_n)} \tag{25}$$

$$dF_a = \frac{dF_s \cos\eta_s \left(\cos\alpha_n \sin\lambda_s + \tan\lambda\left(-\sin\eta_c \cos\lambda_s + \cos\eta_c \sin\alpha_n \sin\lambda_s\right)\right)}{\cos(\phi_n - \alpha_n) - \tan\lambda\cos\eta_c \sin(\phi_n - \alpha_n)}$$

3.3 - Prediction of milling force coefficients

Combining equations (19) and (25), the elementary milling forces dF_t, dF_r, dF_z are

expressed from the shear stress at the exit of the shear band calculated by the oblique cutting model:

$$dF_t = \frac{dz\,t_1\,\tau_h}{\cos\lambda_s \sin\phi_n} \frac{\cos\eta_s\left(\cos\alpha_n \cos\lambda_s + \tan\lambda\left(\sin\eta_c \sin\lambda_s + \cos\eta_c \sin\alpha_n \cos\lambda_s\right)\right)}{\cos(\phi_n - \alpha_n) - \tan\lambda \cos\eta_c \sin(\phi_n - \alpha_n)} = K_{tc}\,dz\,t_1$$

$$dF_r = \frac{dz\,t_1\,\tau_h}{\cos\lambda_s \sin\phi_n} \frac{\cos\eta_s\left(-\sin\alpha_n + \tan\lambda \cos\eta_c \cos\alpha_n\right)}{\cos(\phi_n - \alpha_n) - \tan\lambda \cos\eta_c \sin(\phi_n - \alpha_n)} = K_{rc}\,dz\,t_1 \qquad (26)$$

$$dF_a = \frac{dz\,t_1\,\tau_h}{\cos\lambda_s \sin\phi_n} \frac{\cos\eta_s\left(\cos\alpha_n \sin\lambda_s + \tan\lambda\left(-\sin\eta_c \cos\lambda_s + \cos\eta_c \sin\alpha_n \sin\lambda_s\right)\right)}{\cos(\phi_n - \alpha_n) - \tan\lambda \cos\eta_c \sin(\phi_n - \alpha_n)} = K_{ac}\,dz\,t_1$$

By dividing the cutting forces dF_t, dF_r, dF_z by the chip load $t_1\,dz$ of the ith cutting edge element, the milling cutting force coefficients K_{tc}, K_{rc} and K_{ac} are obtained:

$$\begin{cases} K_{tc} = \dfrac{\tau_h \cos\eta_s\left(\cos\alpha_n \cos\lambda_s + \tan\lambda\left(\sin\eta_c \sin\lambda_s + \cos\eta_c \sin\alpha_n \cos\lambda_s\right)\right)}{\cos\lambda_s \sin\phi_n\left(\cos(\phi_n - \alpha_n) - \tan\lambda \cos\eta_c \sin(\phi_n - \alpha_n)\right)} \\[2ex] K_{rc} = \dfrac{\tau_h \cos\eta_s\left(-\sin\alpha_n + \tan\lambda \cos\eta_c \cos\alpha_n\right)}{\cos\lambda_s \sin\phi_n\left(\cos(\phi_n - \alpha_n) - \tan\lambda \cos\eta_c \sin(\phi_n - \alpha_n)\right)} \\[2ex] K_{ac} = \dfrac{\tau_h \cos\eta_s\left(\cos\alpha_n \sin\lambda_s + \tan\lambda\left(-\sin\eta_c \cos\lambda_s + \cos\eta_c \sin\alpha_n \sin\lambda_s\right)\right)}{\cos\lambda_s \sin\phi_n\left(\cos(\phi_n - \alpha_n) - \tan\lambda \cos\eta_c \sin(\phi_n - \alpha_n)\right)} \end{cases} \qquad (27)$$

During the chip formation, additional shearing takes place in the tertiary deformation zone at the flank of the cutting edge; this mechanism is known as ploughing or rubbing process. To take into account of this process, additional terms have to be added to the previous expressions (27). The force components are thus expressed as a superposition of cutting and rubbing (cutting edge effect), Altintas [27]:

$$\begin{cases} dF_t = (K_{te} + K_{tc}t_1)\,dz \\ dF_r = (K_{re} + K_{rc}t_1)\,dz \\ dF_a = (K_{ae} + K_{ac}t_1)\,dz \end{cases} \qquad (28)$$

The edge force coefficients K_{te}, K_{re} and K_{ae} due to the rubbing forces are introduced as in the mechanistic approach, Altintas [27]. The edge force coefficients K_{te} and K_{re} are usually determined from orthogonal cutting data for a tool-workpiece pair and for appropriate cutting conditions. K_{ae} is known to be very small in oblique cutting, and is often taken as zero, Armarego and Whitfield [13].

$$\begin{bmatrix} dF_x \\ dF_y \\ dF_z \end{bmatrix} = \begin{bmatrix} \sin\varphi & -\cos\varphi & 0 \\ \cos\varphi & \sin\varphi & 0 \\ 0 & 0 & 1 \end{bmatrix} \begin{bmatrix} dF_t(\varphi) \\ dF_r(\varphi) \\ dF_a(\varphi) \end{bmatrix} \qquad (29)$$

Considering the conditions (2-3), the total forces exerted on the tool are obtained by integrating the elementary force components (29) along the axial direction z .

4- Model validation and discussion

The present model was applied to the peripheral milling of a titanium alloy Ti6Al4V, which characteristics are given in Table 1. The experimental results were extracted from a previous work performed by Yucesan and Altintas [9]. Dry up and down milling tests were conducted using single fluted and four-fluted carbide end mills. The cutters have a helix angle α_h of 30° and a diameter of 19.06 mm. The spindle speed ω was equal to 500 rev/min for all the experiments; various values of rake angle and of feed rake were tested, see Table 2.

Table 1 – Characteristics of the Ti6Al4V titanium alloy

Density ρ (kg/m³)	Heat capacity c (J/kg.°K)	Thermal conductivity k (W/m.°K)
4430	526	7

Table 2 – Cutting conditions

Spindle speed ω (rev/min)	Radial depth of cut d_r (mm)	Axial depth of cut d_a (mm)	Feed rate per tooth f_t (mm)	Radial rake angle α_r (°)
500	Full and half immersion	5.08 and 7,5 mm	0.0127, 0.0254, 0.0508 and 0.2032	0, 5 and 12

The parameters of the Johnson-Cook law (9) for the Ti6Al4V alloy were deduced from the previous work of Meyer and Kleponis [28] , they are given in Table 3.

Table 3 – Johnson-Cook parameters for Ti6Al4V

A (MPa)	B (MPa)	$\dot{\gamma}_0$ (s⁻¹)	n	m		Reference temperature T_r (°K)	Melting temperature T_m (°K)
862	331	1	0.34	0.012	0.80	296	1950

According to the work of Armarego [12, 13], Yucesan and Altintas [9], Budak [1] proposed to determine the edge force coefficients K_{te} and K_{re} from semi-orthogonal experiments conducted. During the tests, the measured forces were due to shearing (chip formation) and ploughing or rubbing at the flank of the cutting edge. The coefficients K_{te} and K_{re} represent the ploughing/rubbing parts of the cutting and feed measured forces per unit width of cut. The values $K_{te} = 24\,N/mm$ and $K_{re} = 43\,N/mm$ were found for the Ti6Al4V titanium alloy. From the measured forces, the mean friction angle λ was also determined, it was found depending on the rake angle:

$$\lambda = 19.1 + 0.29\,\alpha_n\,(\deg.) \tag{30}$$

In the present work, the primary shear zone thickness was taken as $h = 10\,\mu m$ according the experimental study of Molinari et al. [29] and the normal shear angle was supposed to be given by the Merchant law.
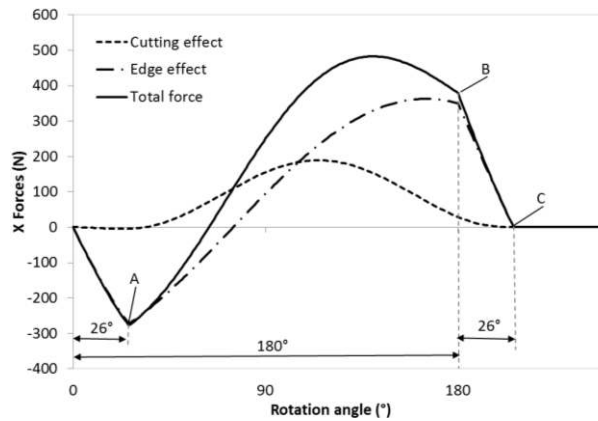

Fig. 5. Predicted cutting forces for full immersion. Single-flutted endmill, feed rate $f_t = 0.0127\,mm/tooth$, axial depth of cut $d_a = 7.5mm$, rake angle $\alpha_r = 0$ and cutting speed $V = 30\,m/min$.

Before discussing about the validation of the modeling approach, it is interesting to present a first result of the model calculation. Single-flutted endmill in full immersion is considered, and only the X-force calculated signal is presented figure 5. The edge effect, the cutting effect, and their resulting effects are separately shown in this figure, obtained from relations (28) and (28) integrated all along the working cutting edge. Through this X-Force signal, the tooth engagement may be decomposed into three stages OA, AB and BC. The first stage OA corresponds, according the helix angle α_h, to the input process of the tooth into the workpiece from $z = 0$ to $z = d_a$ (axial depth of cut), and the associate

rotation angle is $d_a \tan \alpha_h / R$, where R is the tool radius. During this stage, the chip thickness, given by the relation (4), is very small and the edge effect is predominant. From point A to point B, the tooth of the tool is working all over the depth of cut, and edge effect and cutting effect are combined. The point C is the beginning of the ouput process of the tooth from the workpiece; and in the same manner as in the first stage, the chip thickness is small and the edge effect is predominant. These three stages are visible in the following experimental results.

The influence of the radial rake angle α_r (or normal rake angle $\alpha_n = \tan^{-1}(\cos \alpha_h \tan \alpha_r)$) on the cutting forces components F_x, F_y and F_z is first discussed. The angle α_r influences the cutting forces via the normal shear angle ϕ_n, relation (18). In addition, the rake angle α_r affects the temperature and the pressure distributions along the tool-chip and modifies the repartition of sticking and sliding zones in this interface. These effects are globally taken into account through the introduction of a mean friction coefficient (or angle) and by the relationship (30).

Experimental and predicted forces are reported in Fig. 6 for full immersion milling tests, and three values of radial rake angle $\alpha_r = 0, 5, 12°$. From experiments, the dependency of forces on the rake angle is more evident for rake angle range from 0 to 5 °; this tendency is not retrieved with the proposed model as it was not with the Yucesan and Altintas [9] approach. This discrepancy may be perhaps attributed to a lack of description of the contact conditions on rake face or to tool deflection. When α_r becomes smaller, the shear angle decreases, and this causes an increase in the length of primary shear zone. As a consequence, the thickness of the chip and the length of the tool-chip contact become larger, leading to an increase of cutting forces; and when the cutting forces are large enough tool deflection appears. This tool deflection modifies the engagement duration of the tool; from experimental results, it appears that for $\alpha_r = 0$ the engagement duration of the helical flute is greater than for $\alpha_r = 5 \ and \ 12°$.
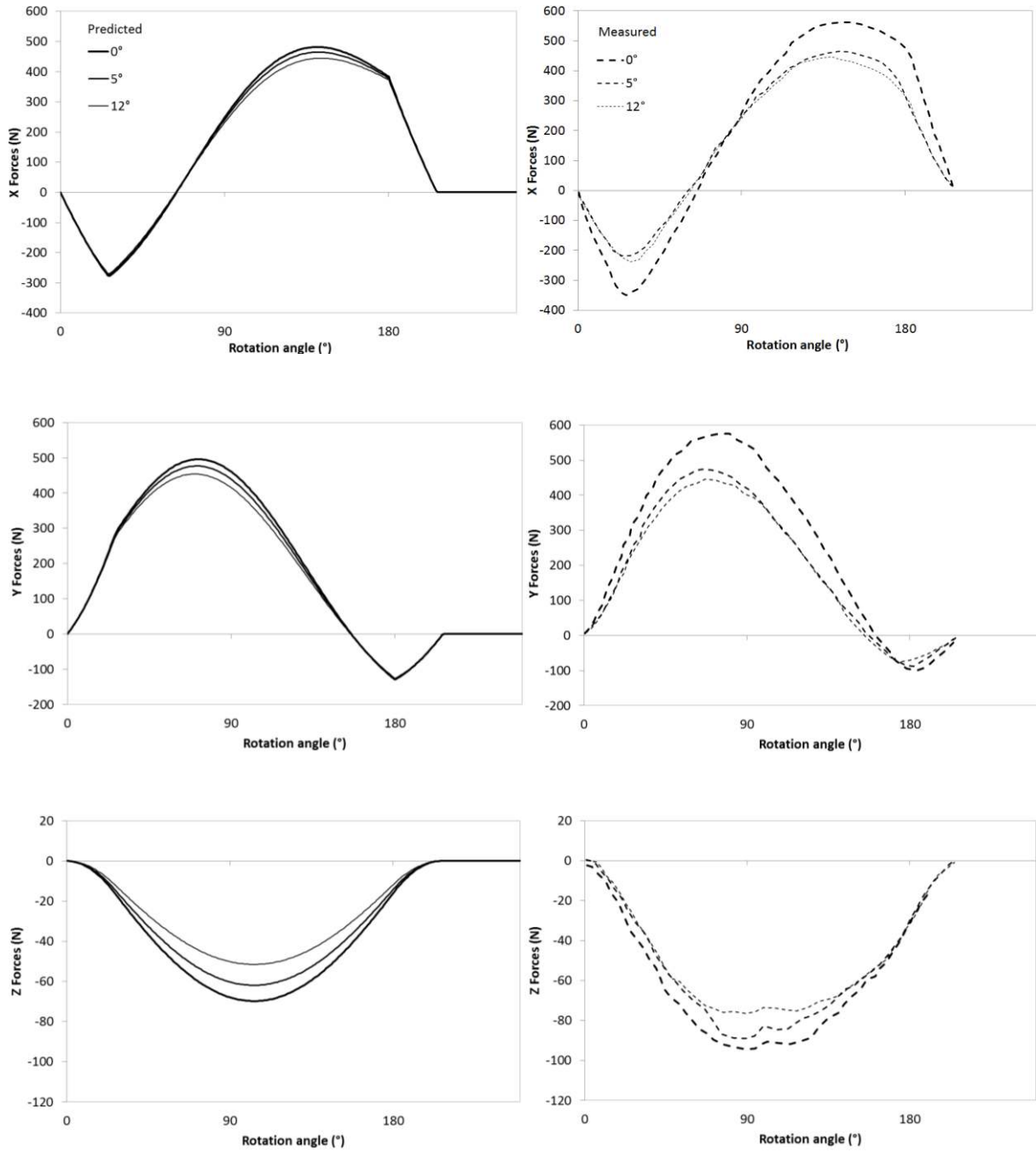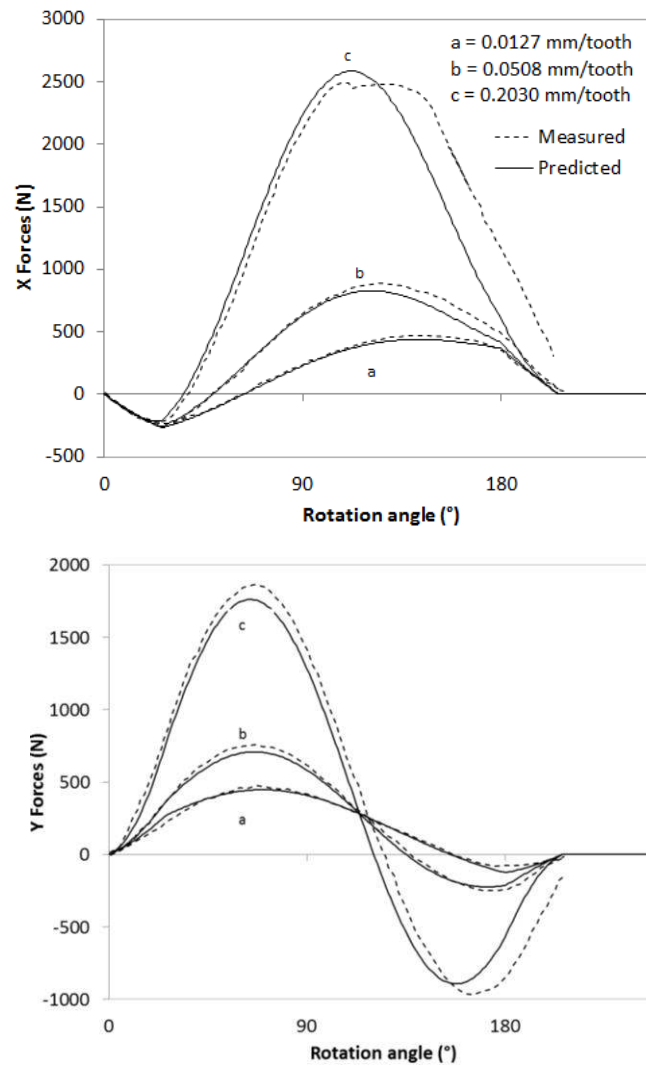
Fig. 6. Measured (from Yucesan and Altintas [9]) and predicted cutting forces for full immersion tests and for various rake angle values $\alpha_r = 0$, 5° and 12° . Single-flutted end mill, feed rate $f_t = 0.0127mm/tooth$, axial depth of cut $d_a = 7.5mm$, cutting speed $V = 30\ m/min$.

According to the orthogonal tests data performed in the work of Armarego [12, 13], Yucesan and Altintas [9], Budak [1] the mean friction coefficient $\bar{\mu}$ can be supposed constant over a wide range of cutting conditions for the present tool-workpiece pair. In the following, the mean friction angle λ was taken constant $\lambda = 26°$ ($\bar{\mu} = 0.48$).

The evolution of the cutting forces in terms of the feed rate f_t is reported in the Fig. 7 for full immersion milling with a comparison between the present model and the experimental results. The cutting forces are accurately predicted by the predictive approach; however, the difference between the model calculation and the tests data becomes more significant for the greater value of feed per tooth $f_t=0.203$ mm/tooth. In the same way as for $\alpha_r = 0$, this difference can be attributed to tool deflection which may appear when the cutting forces are large enough.
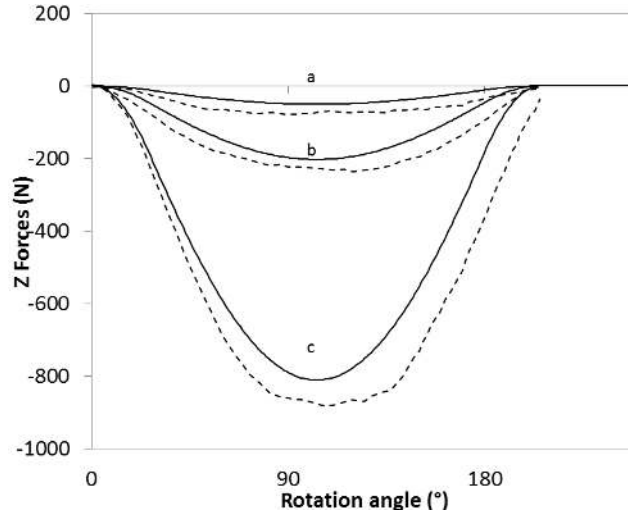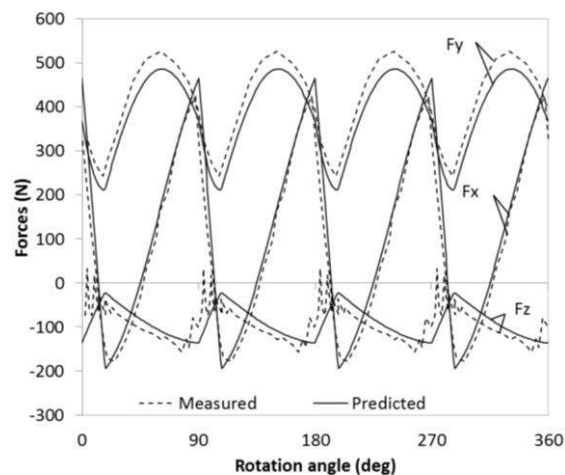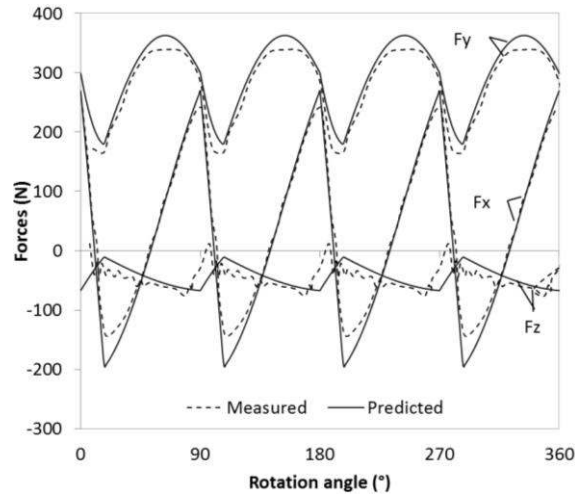
Fig. 7. Measured (from Yucesan and Altintas [9]) and predicted cutting forces for full immersion tests and various feed rate value, f = 0.0127, 0.0508, 0.203 mm/tooth. Single-flutted end mill, rake angle $\alpha_r = 12°$, axial depth of cut $d_a = 7.5mm$, spindle speed N=500 rev/min or cutting speed V= 30m/min.

Fig. 8 compares the calculated and the experimental results, for half-immersion up-milling and half-immersion down-milling tests. The model predictions are in good agreement with the measured forces. The values of shear stress τ in the primary shear zone predicted by the model are very close to those found by Yucesan and Altintas [9] from orthogonal cutting tests. In the same way, Yucesan and Altintas [9] measured the chip flow angle; the obtained values were in the range $15° < \eta_c < 20°$, lower than the helix angle (which was equal to 30°,for all the endmills used during the experiments). With the proposed model, the chip flow angle was calculated from equation (23); and, the obtained values were $16° < \eta_c < 21°$, in agreement with experimental results. This demonstrates also that the Stabler rule is not valid for the chip flow angle calculation ($\eta_c = \lambda_s = 30°$).

(a) Up milling, f= 0.0508 mm/tooth, $\alpha_r = 12°$

19

(b) Up milling, f= 0.0254 mm/tooth, $\alpha_r = 12°$
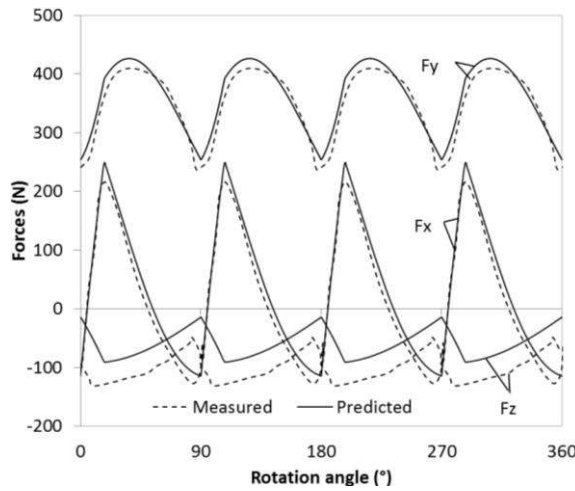
(c) Down milling, f= 0.0254 mm/tooth, $\alpha_r = 0°$

Fig. 8. Measured (from Yucesan and Altintas [9]) and predicted cutting forces for up and down milling half immersion tests. Four-flutted end mill, axial depth of cut $d_a = 5.08mm$, spindle speed N=500 rev/min or cutting speed V= 30m/min.

5- Conclusions

In this paper, a thermomechanical model of oblique cutting, based on an analytical approach, was applied to the end milling process. For an infinitesimal cutting edge element, the elementary chip is obtained from an oblique cutting process where the chip formation was supposed to occur mainly by shearing within a thin zone, the primary shear band. The material flow through this band was assumed to be stationary and modelled by using a one-dimensional approach. The material characteristics such as strain rate sensitivity, thermal softening and strain hardening were considered. Thermomechanical

coupling and the inertia effects were accounted for. The chip flow angle was determined by the assumption that the friction force on the tool rake face is collinear to the chip flow direction; this leads to a non linear equation which was solved by using the Newton-Raphson method.

The predicted cutting forces are in good agreement with experimental data over a wide range of cutting conditions. It can be noted that although the present model was established for stationary conditions and for continuous chips, it gives acceptable predictions for segmented chip as in milling of titanium alloy. The present predictive model can represent a real alternative to the classical mechanistic approach which requires many experimental tests for a given pair of tool-workpiece materials and for a given cutter geometry.

References

[1] Budak E, Altintas Y, Armarego EJA. Prediction of milling force coefficients from orthogonal data. Journal of Manufacturing Science and Engineering 1996; 118: 216-224.

[2] Martelotti ME. An analysis of milling process. Transactions of ASME 1941; 63:677-700.

[3] Koenigsberger F, Sabberwal AJP. An investigation into the cutting force pulsations during milling operations. International Journal of Machine tool Design and Research 1961; 1: 15-33.

[4] Tlusty J, MacNeil P. Dynamics of cutting forces in end milling. Annals of CIRP 1975; 24 (1): 21-25.

[5] Kline WA, DeVor RE, Zdeblick WJ. A mechanistic model fort he force system in end milling with application to machining airfarames structures. Proc. of the 8th North American Manufacturing Res Conf. 1980; 8: 297.

[6] Kline WA, DeVor RE. The effect of runout on cutting geometry and forces in end milling. International Journal of Machine tool and Research 1983; 23 (2/3): 123-140.

[7] Sutherland J, DeVor RE. An improved method for cutting force and surface error prediction in flexible end milling systems. Journal of Engineering for Industry, Transactions of the ASME 1986; 108: 269-279.

[8] Altintas Y, Spence A. End milling force algorithms for CAD systems. Annals of the CIRP 1991; 40(1): 31-34.

[9] Yucesan G, Altintas Y. Improved modelling of cutting coefficients in peripheral milling. International Journal of Machines Tools Manufacturing 1994; 34 (4): 473-487.

[10] Dang JW, Zhang WH. Cutting force modeling for flat end milling including bottom edge cutting effect. International journal of Machine Tools & Manufacture 2010; 50: 986-997.

[11] Wang M, Gao L, Zheng Y. An examination of the fundamental mechanics of cutting force coefficients. International journal of Machine Tools & Manufacture 2014; 78: 1-7.

[12] Armarego EJA, Brown RH. The machining of metals. Prentice Hall , New York, 1969.

[13] Armarego EJA, Whitfield RC. Computer based modelling of popular machining operations for forces and power prediction. Annals of the. CIRP 1985; 34(1): 65-69.

[14] Armarego EJA, Deshpande NP. Computeriezd Cutting models for forces in end milling including eccentricity effects. Annals of the CIRP 1989; 38 (1): 45-49.

[15] Oxley PLB. An analytical approach to assessing machinability. Ellis Horwood, 1989.

[16] Li HZ, Zhang WB , Li XP. Modelling of cutting forces in helical end milling using a predictive machining theory. International Journal of Mechanical Sciences 2001; 43 (8):1711-1730.

[17] Li HZ,. Li XP. Milling force prediction using a dynamic shear length model. International Journal of Machine Tools and Manufacture 2002; 42 (2):277-286.

[18] Moufki A , Dudzinski D, Molinari A, Rausch M. International Journal of Mechanical Science, Thermoviscoplastic modelling of oblique cutting: forces and chip flow predictions. International Journal of Mechanical Sciences 2000; 42 (6): 1205-1232.

[19] Moufki A , Devillez A, Dudzinski D, Molinari A. Thermomechanical modelling of oblique cutting and experimental validation. International Journal of Machine Tools and Manufacture 2004; 44 (9): 971-989.

[20] Bahi S, Nouari M, Moufki A, El Mansori M, Molinari A. A new friction law for sticking and sliding contacts in machining. Tribology International 2011; 4 (7–8): 764-771.

[21] Bahi S, Nouari M, Moufki A, El Mansori M, Molinari A. Hybrid modelling of sliding–sticking zones at the tool–chip interface under dry machining and tool wear analysis. Wear 2012; 286–287: 45-54.

[22] Zorev NN, Massey HSH. Metal cutting mechanics. Pergamon Press, 1966.

[23] Trent EM, Wright PK. Metal Cutting. Fourth edition, Butterworth-Heinemann publications, 2000.

[24] Ackroyd B, Chandrasekar S, Compton WD. A model for the contact conditions at the chip–tool interface in machining. Transactions of the ASME 2003;125: 649–60.

[25] Asthakov PV. Tribology of metalcutting. Tribology and Interface Engineering Series 2006;52:124–212.

[26] Filice LMF, Rizzuti S, Umbrello D. A critical analysis on the friction modelling in orthogonal machining. International journal of Machine Tools & Manufacture 2007; 47: 709-714.

[27] Altintas Y. Manufacturing Automation: Metal Cutting Mechanics, Machine Tool Vibrations, and CNC Design. Cambridge University Press, 2000.

[28] Meyer HW, Kleponis DS. Modeling the high strain rate behaviour of titanium undergoing ballistic impact and penetration. Int. J. of Impact Engineering 2001; 26: 509-521.

[29] Molinari A, Musquar C, Sutter G. Adiabatic shear banding in high speed machining of Ti–6Al–4V: experiments and modelling. International Journal of Plasticity 2002; 18: 443–459.